Bone 92 (2016) 18–28

Contents lists available at ScienceDirect

Bone

journal homepage: www.elsevier.com/locate/bone

Full Length Article

Conditional deletion of IGF-I in osteocytes unexpectedly accelerates bony union of the fracture gap in mice

K.-H. William Lau [a,b], Charles H. Rundle [b], Xiao-Dong Zhou [a], David J. Baylink [a], Matilda H.-C. Sheng [a,*]

[a] Division of Regenerative Medicine, Department of Medicine, Loma Linda University School of Medicine, Loma Linda, CA, USA
[b] Musculoskeletal Disease Center, Jerry L. Pettis Memorial VA Medical Center, Loma Linda, CA, USA

ARTICLE INFO

Article history:
Received 22 February 2016
Revised 3 August 2016
Accepted 8 August 2016
Available online 9 August 2016

Keywords:
Fracture repair
Insulin-like growth factor-I
Osteocytes
Conditional deletion
Intramembranous bone formation
Endochondral bone remodeling
Bony union
Transgenic mice

ABSTRACT

This study evaluated the effects of deficient IGF-I expression in osteocytes on fracture healing. Transgenic mice with conditional knockout (cKO) of *Igf1* in osteocytes were generated by crossing *Dmp1*-Cre mice with *Igf1* flox mice. Fractures were created on the mid-shaft of tibia of 12-week-old male cKO mice and wild-type (WT) littermates by three-point bending. At 21 and 28 days post-fracture healing, the increases in cortical bone mineral density, mineral content, bone area, and thickness, as well as sub-cortical bone mineral content at the fracture site were each greater in cKO calluses than in WT calluses. There were 85% decrease in the cartilage area and >2-fold increase in the number of osteoclasts in cKO calluses at 14 days post-fracture, suggesting a more rapid remodeling of endochondral bone. The upregulation of mRNA levels of osteoblast marker genes (*cbfa1*, *alp*, *Opn*, and *Ocn*) was greater in cKO calluses than in WT calluses. μ-CT analysis suggested an accelerated bony union of the fracture gap in cKO mice. The *Sost* mRNA level was reduced by 50% and the *Bmp2* mRNA level was increased 3-fold in cKO fractures at 14 days post-fracture, but the levels of these two mRNAs in WT fractures were unchanged, suggesting that the accelerated fracture repair may in part act through the Wnt and/or BMP signaling. In conclusion, conditional deletion of *Igf1* in osteocytes not only did not impair, but unexpectedly enhanced, bony union of the fracture gap. The accelerated bony union was due in part to upregulation of the Wnt and BMP2 signaling in response to deficient osteocyte-derived IGF-I expression, which in turn favors intramembranous over endochondral bone repair.

1. Introduction

Bone has an amazing ability to regenerate itself without a scar after injuries, such as fractures. The repair of long bone fractures is mediated by endochondral bone repair, which is divided into four major overlapping stages: 1) the initial inflammatory response, 2) the formation of soft callus, 3) the formation of hard callus, and 4) the bone remodeling and bony union of the fracture gap [1]. The remodeling phase involves resorption of cartilage and conversion of the cancellous callus bone into cortical bone that is indistinguishable from native bone. This phase also includes neovascularization to re-establish blood flow to the fracture site [2]. The mechanism responsible for fracture repair is highly complex and involves actions of the various cell types (including osteoblasts, osteoclasts, chondrocytes, osteocytes, endothelial cells, and mesenchymal stem cells) through local expression of the variety of growth factors and signaling molecules that lead to coordinated development of cartilaginous callus, bony remodeling of the callus, bony union of the gap, and the eventual restoration of the bone structure and strength.

The osteocyte, which is the most abundant cell type in the cortical bone, has an extensive network of dendrites extending to and making contact with other osteocytes, periosteal and endosteal lining cells, bone surface osteoblasts and osteoclasts, and bone marrow cells through a widespread, interconnected canaliculi system [3]. This network of canaliculi allows soluble osteocyte-derived paracrine signaling molecules to migrate freely from the osteocyte to act on other bone cells [4]. Hence, the osteocyte is strategically well positioned within the bone matrix to sense physical and biochemical signals that regulate bone metabolism, remodeling, and local regeneration. There is now increasing evidence that the osteocyte and its secretory factors, such as sclerostin (*Sost*), may play key regulatory roles in fracture repair. For instance, earlier studies have suggested that surviving osteocytes at fracture sites are important for robust cellular recruitment of the various cell types and the release of osteopontin during the initial phase of fracture healing [5] and that osteocytes participate in the periosteal callus cartilage formation and bone regeneration during fracture healing [6]. More recent studies have shown that during hip fracture healing, the expression of *Sost* by osteocytes at the fracture site was downregulated [7]. Mice lacking the *Sost* gene accelerated fracture healing [8,9].

* Corresponding author at: Division of Regenerative Medicine, Department of Medicine, Loma Linda University School of Medicine, 11234 Anderson Street, Loma Linda, CA 92350, USA.
E-mail address: MSheng@llu.edu (M.H.-C. Sheng).

http://dx.doi.org/10.1016/j.bone.2016.08.005
8756-3282/

Administration of the sclerostin neutralizing monoclonal antibody enhanced fracture repair and bone strength [10–14]. There is also evidence that conditional deletion of the connexin 43 gene in osteocytes delayed bone formation and impaired fracture repair [15].

We are interested in the regulatory role of osteocyte-derived IGF-I in fracture repair for the following reasons: first, fracture repair requires bone regeneration, and IGF-I promotes bone formation, regeneration, and fracture repair [16,17]. Second, the expression and bone cell production of IGF-I were greatly increased at the fracture site during the early healing phase [18,19]. Third, IGF-I is a key mediator of the skeletal response to PTH [20], which has shown to promote fracture healing [16,21]. Fourth, local IGF-I treatment [17,22] or systemic treatment with IGF-I-expressing mesenchymal stromal cells [23,24] promoted fracture healing in a number of animal models. Moreover, it is generally accepted that moderate axial mechanical loading enhances fracture repair by stimulating formation of periosteal callus and increases the rate of healing [25–28]. Conditional disruption of *Igf1* gene in osteocytes completely abolished the bone formation response to mechanical loading [29]. Accordingly, we anticipate that deficient expression of osteocyte-derived IGF-I would also impede the fracture repair process.

In this study, we sought to test the hypothesis that osteocyte-derived IGF-I plays an essential role in fracture repair by comparing the healing of a simple closed tibial fracture in osteocyte *Igf1* conditional knockout (cKO) mice with that in wild-type (WT) littermates. Surprisingly, this study shows that conditional deletion of *Igf1* in osteocytes not only did not impede, but in fact promoted, fracture callus remodeling and accelerated bony union of the fracture gap. These unexpected findings indicate that osteocyte-derived IGF-I may have a novel inhibitory role in fracture repair.

2. Materials and methods

2.1. Animals

All animal procedures were reviewed and approved by the Institutional Animal Care and Use Committee (IACUC) of the Loma Linda University and also by the Animal Care and Use Review Office (ACURO) of the Department of the Army of the United States. In conducting research using animals, the investigators adhered to the Animal Welfare Act Regulations and other Federal statutes relating to animals and experiments involving animals and the principles set forth in the current version of the guide for *Care and Use of Laboratory Animals*, National Research Council. With the exception of μ-CT analyses that were performed at the Jerry L. Pettis Memorial VA Medical Center (Loma Linda, CA, USA), all experiments were carried out in the AALAC accredited Animal Care Facility and the laboratory space of the Department of Medicine of the Loma Linda University. Animals were housed in groups of 4 per cage under a 12-h light/dark cycle and provided water and regular rodent chow ad libitum.

Osteocyte *Igf1* cKO mice were generated by crossing *Igf1*$^{flox/flox}$ mice with *Dmp1*-Cre mice as previously described [30]. Briefly, the *Dmp1*-Cre mice (in mixed genetic background of 50% C57BL/6 and 50% CD1) were first bred with the *Igf1*$^{flox/flox}$ mice (in C57BL/6 genetic background) to generate heterozygous mice with the genetic background of *Igf1*$^{flox/-}$/*Dmp1*-Cre at F1 generation (all with a mixed genetic background of 75% C57BL/6 and 25% CD). The F1 heterozygous mice were then crossbred with each other to produce 25% homozygous cKO mice (*Igf1*$^{flox/flox}$/*Dmp1*-Cre), 50% heterozygous cKO mice (*Igf1*$^{flox/-}$/*Dmp1*-Cre), and 25% WT littermates (*Igf1*$^{-/-}$/*Dmp1*-Cre). Only male homozygous cKO mice and WT littermates were used for this study.

2.2. Closed tibial mid-shaft fractures

Standard transverse closed fractures were produced on the cortical cortex at the midshaft of the right tibiae (above the tibiofibular junction) of 12-week-old male mice by the three-point bending technique as previously described [31]. The left tibiae served as respective internal intact controls. Briefly, animals were anesthetized by isoflurane inhalation. A mid-line skin incision over the knee joint was made to gain access to the proximal tibial metaphysis, and a pilot hole was made using a 30-gauge needle at a position just medial to the patella tendon. A stainless steel pin (25-gauge) was inserted into the intramedullary space of the tibia for internal fixation and fracture stabilization. A smaller pin (27-gauge) was used for cKO mutant mice due to their 8–12% smaller bone size than WT mice [30]. The appropriate placement of the pin was confirmed by X-ray. The exposed end of the pin was cut proximally at the level of the bone. Wounds were closed with surgical sutures, and the tibia was held in a fixed position. A single complete fracture was then created by three-point bending using an Instron Mechanical tester (Norwood, MA). Fracture bones were harvested for the examination of fracture healing at 14, 21, and 28 days post-fracture, because endochondral bone repair and remodeling are maximal at these time points [2,32,33]. Early time points were not examined because we were interested in the functional aspects of the healing (i.e., callus remodeling and bony union). Fracture healing was assessed by X-ray, pQCT, μ-CT, histology, histomorphometry, and gene expression analyses.

2.3. Peripheral quantitative computed tomography (pQCT) analysis

Fractured tibiae after dissection were immediately fixed in 10% formalin overnight and were stored in phosphate buffer saline at 4 °C until analyses. The area of the tibiae corresponding to the fracture calluses was scanned and analyzed by the pQCT (STRATEC XCT). The outer and inner thresholds were set at 230 and 630 mg/cm^3 to distinguish the woven and cortical bone compartments, respectively. The scanned bone slides were analyzed with a software program (version 6.00) provided by the manufacturer.

2.4. Micro-computed tomography (μ-CT) analysis

Micro-CT analysis of fracture healing was accomplished using a Scanco *Viva*-CT 40 instrument. Scans were performed at 55 keV, and the analysis of the fracture calluses was conducted using density thresholds that resolved the higher density native cortical bone (570–1000 mg/cm^3 HA) from the lower density callus woven bone (220–570 mg/cm^3 HA). This approach might include some intramedullary trabecular bone, which is expected to be minimal at the midshaft where the fracture is produced.

2.5. Torsional bone strength measurement

The fractured tibia at 21 days post-fracture and corresponding contralateral tibia were torsion tested for torsional stiffness using an Instron 55MT1 rotary tester. Briefly, the epiphyses were cast into a dental resin that adheres to the bone and allowed each end of the tibia to be secured in the opposing jaws of the torsional tester. Torsional force was applied at 1°/s until failure. Torsional stiffness (in N-mm/°), which was used as a measure of torsional bone strength, was calculated from the linear portion of the force vs angle curve prior to the yield point. To normalize for the 8–12% smaller bone size seen in cKO mutants, the relative return of torsional bone strength to pre-injury strength of each fractured bone was shown as the ratio of torsional stiffness of the fractured bone to that of the contralateral intact bone. A ratio of 1.0 indicates the full return of its torsional strength.

2.6. Bone histology

Briefly, the isolated bone section containing the fracture callus was immersion-fixed in ice-cold 4% paraformaldehyde for 16 h. After the removal of surgical pins, specimens were decalcified in 14% EDTA for 3-4 weeks at 4 °C with changes of decalcification solution every two

days. Muscle and connective tissues surrounding the bone were not completely removed in order to preserve cellular structures at the periosteal surface of the bones. Tissue was subsequently infiltrated, embedded into paraffin wax, and sectioned using a Leica Microtome. Paraffin-embedded sections of 5 μm in thickness were kept at 4 °C until staining. The fracture callus was examined for evidence of cartilage formation by Alcian blue staining and also by Masson's trichrome staining. Cartilage area in fracture calluses was quantified as percentage of the total callus area in the Alcian blue (or Masson's trichrome) stained sections using the OsteoMatrics software. Measurements were performed in a blinded manner to avoid unintended biases.

2.7. Periosteal bone formation parameters

Tetracycline and demeclocycline were injected into animals on 8 and 2 days, respectively, prior to euthanasia as previously described [34]. At euthanasia, the fractured tibiae were isolated, cleaned and fixed with formalin. The formalin-fixed bone was then dehydrated in ethanol and embedded into methylmethacrylate. The cross-sections (80–100 μm in thickness) of the region corresponding to the fracture callus, marked by a pencil, were prepared by Precision Diamond Wire Saw (Delaware Diamond Knives, Wilmington, DE) and cover slipped in 70% glycerol for measurements of periosteal bone formation parameters, which were obtained with an Olympus fluorescent microscope BX51 (Tokyo, Japan) and the Osteomeasure digitalized system (OsteoMetrics, GA).

2.8. Quantitative real-time PCR (qRT-PCR) for gene expression

Briefly, the fracture site and corresponding region of the contralateral intact tibia were each pulverized under liquid nitrogen and stored at −80 °C until use. Total RNA was extracted using the RNeasy mini kit (Qiagen, Valencia, CA). The RNA quality was assessed by an Agilent 2100 Bioanalyzer and Agilent 2100 Expert Software (Santa Clara, CA). Total RNA was immediately reverse-transcribed into cDNA using a commercial kit (Invitrogen). The SYBR Green-based qPCR reaction was performed with a commercial kit (Applied Biosystems) in an ABI 7500/7500 Fast Real Time PCR System (Applied Biosystems, Foster City, CA). Each PCR was run in duplicate according to the standard protocol provided by ABI. The sequence of the PCR primer set of each test gene is shown in Supplemental Table S1.

2.9. Statistical analysis

The group size was determined by power analysis, based on standard deviation estimates from μ-CT measurements in previous studies of similar nature. The group size of 6–8 mice would detect a 20% difference in trabecular bone parameters between the test and control groups. Results are shown as means ± standard error of the mean (SEM). Statistical significance was determined by two-tailed Student's *t*-test with uneven sample size. A difference was considered significant, when $P < 0.05$.

3. Results

3.1. Conditional deletion of Igf1 in osteocytes did not affect basal cortical and trabecular bone densities

Before we initiated fracture studies in osteocyte *Igf1* cKO mice, we compared basal cortical bone parameters at the mid-shaft as well as basal trabecular bone parameters at the proximal metaphysis of intact tibiae of cKO mice with those of WT littermates by μ-CT. Consistent with the previous reports [29,30,35], the femur length of male osteocyte *Igf1* cKO mice at 12 weeks of age was 4.6% shorter than that of corresponding male WT littermates (Fig. 1A). The total cortical tissue (Ct·TV) and bone volume (Ct·BV) in these cKO mice were each reduced by 25%, resulting in no differences in Ct·BV/TV between the two mouse strains (Fig. 1B). Similarly, despite the significant reduction in both Tb·TV and Tb·BV in cKO mice, there were no significant differences in Tb·BV/TV, Conn-Dens, Tb·N, Tb·Th, or Tb·Sp between the two mouse strains (Fig. 1C). Thus, deficient *Igf1* expression in osteocytes did not alter basal cortical and trabecular bone densities or trabecular architecture.

3.2. Igf1 osteocyte cKO mutant mice formed smaller fracture calluses than WT mice

To monitor the healing of tibial fractures in *Igf1* cKO mutant mice and in WT littermates, we first followed the time course of the healing by X-ray densitometry (Fig. 2A). All six WT mice, but only one of the six cKO mice, still showed clear X-ray evidence for the fracture gap at 28 days post-fracture. The average size of mineralized fracture calluses in cKO mice at 21 days and 28 days post-fracture (measured by pQCT) was significantly smaller than that in WT calluses by 16% and 12%, respectively (Fig. 2B).

To confirm the smaller callus size, the volume of mineralized calluses of cKO and WT mice at 21 days post-fracture was determined by μ-CT. The total bony callus volume of cKO mice was smaller than that of WT littermates by >40% (Fig. 3A). When bone mineral content (BMC) within the fracture calluses was separated into lower-density (220–570 mg/cm^3 HA) woven bone and higher-density (570–1000 mg/cm^3 HA) cortical bone, the bone volume in each sub-fraction within fracture calluses of cKO mice was significantly less than that of corresponding sub-fraction of WT littermates (Fig. 3B). Intriguingly, despite the smaller callus volume, the average bone mineral density (BMD) in the fracture callus of cKO mice was significantly higher than that of WT littermates (Fig. 3C). Three-dimensional reconstruction of the longitudinal, midline cut-away view of healing fractures at 21 days post-fracture confirms that there was indeed more newly formed lower-density (220–570 mg/cm^3 HA) callus woven bone (shown in yellow color) as well as more higher-density (570–1000 mg/cm^3 HA) cortical bone (shown in white color) in cKO mice than in WT fractures (Fig. 3D). Thus, mice with deficient *Igf1* expression in osteocytes formed significantly smaller but denser bony calluses than WT littermates during fracture healing.

3.3. Fractures of Igf1 osteocyte cKO mice had less callus cartilage than WT fractures

The formation and subsequent bony remodeling of the cartilaginous callus are two key phases of endochondral bone repair [1]. To evaluate the effects of deficient expression of *Igf1* in osteocytes on the amount of cartilaginous callus, we histochemically stained cartilaginous callus on longitudinal thin sections of the fracture site of cKO and of WT calluses at 14 days post-fracture with Alcian blue that stains proteoglycan, a major component of cartilage. There was relatively little cartilage (occupying only >5% of the total callus area) in cKO calluses, while >30% of the callus area in WT fractures was occupied by cartilage (Fig. 4A). The cKO calluses also showed >80% reduction each in the abundance of *Col2α1* mRNA (Fig. 4B) and *Col10α1* mRNA (Fig. 4C) [two well-known marker genes of cartilage] than WT calluses. Thus, cKO fractures formed significantly less callus "cartilage-like" tissues than WT fractures during the early healing phase, suggesting that endochondral bone formation was greatly reduced and/or endochondral remodeling was enhanced in cKO fractures compared to WT fractures.

3.4. Conditional disruption of Igf1 in osteocytes enhanced bony remodeling of callus cartilage

To evaluate whether cKO fractures also exhibited an increased remodeling of the cartilaginous callus, we counted and compared the number of tartrate-resistant acid phosphatase (TRAP)-positive, multinucleated, osteoclasts in the calluses of cKO mutants with those of WT

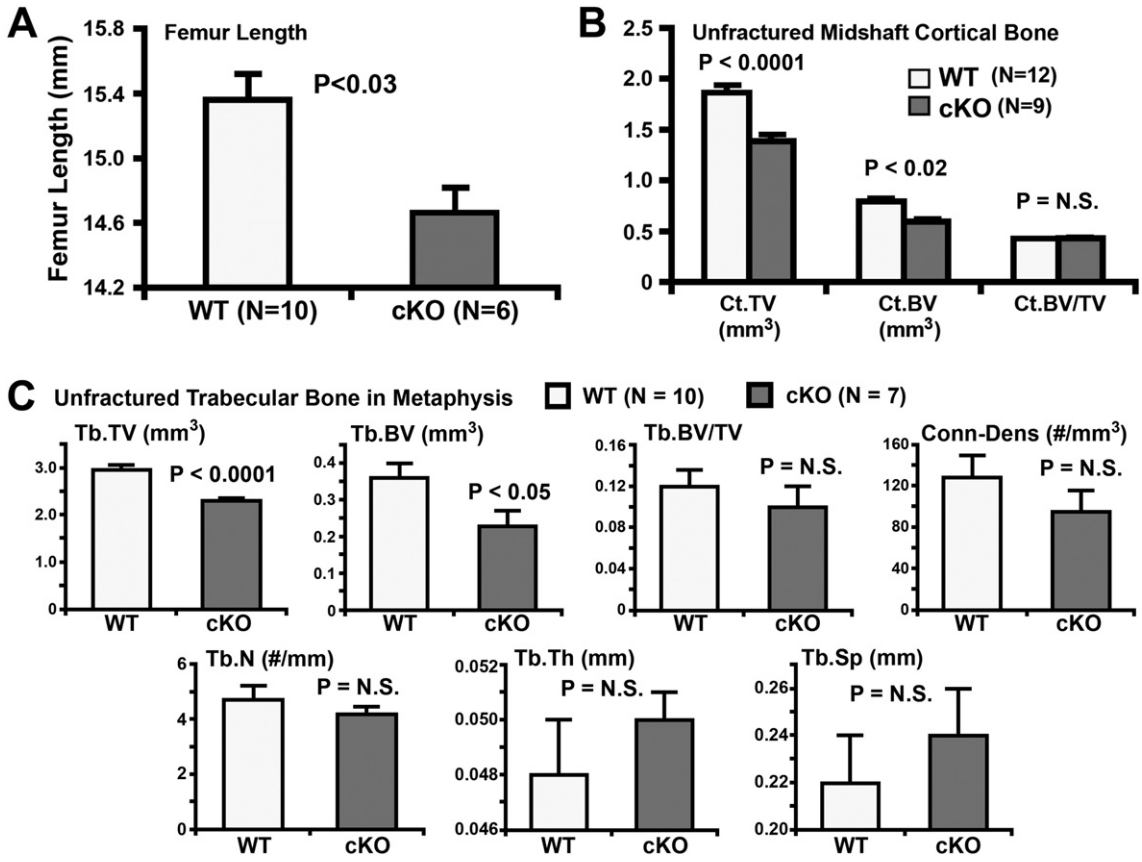

Fig. 1. Comparison of femur length (A), and tibial basal cortical (B) and trabecular (C) bone parameters of 12-week-old male adult osteocyte *Igf1* cKO mice with those of age- and gender-matched WT littermates. Femur length was measured with a digital caliper. Cortical and trabecular bone parameters were determined by μ-CT at the midshaft and proximal metaphysis of the tibia, respectively. N.S. = not significant ($P > 0.05$).

littermates at 14 days post-fracture. There was significantly greater TRAP-stained area in cKO fracture calluses than in WT control calluses (Fig. 5A). This increase was accompanied by ~35% increase in the number of osteoclasts per mm^2 callus surface (Fig. 5B). The qRT-PCR analysis confirmed the three- to fourfold increase in *Acp5b* mRNA level in cKO calluses compared to WT calluses (Fig. 5C). Thus, the cKO fractures also had an accelerated bony remodeling of fracture cartilage-like tissues compared to WT fractures.

3.5. Igf1 osteocyte cKO mutants did not show detectable reduction in IGF-I expression in chondrocytes within the fracture callus

Inasmuch as the 10-kb *Dmp1* promoter is considered to be a promoter specific for osteocytes or late osteoblasts [36–41], this promoter is "leaky" in that the *Dmp1*-Cre-mediated recombination has also been reported to occur in the brain and muscle of the cKO mice [30,36]. Chen et al., [42] have also recently reported that weak Cre recombinase expression was found in growth plate chondrocytes of their conditional constitutive activated β-catenin transgenic mice generated with the same *Dmp1*-Cre mice, suggesting that the *Dmp1*-Cre-mediated recombination might also occur in chondrocytes. Because IGF-I plays an important role in maintaining normal growth and differentiation of growth plate chondrocytes, there is the possibility that the observed reduction in the amounts and accelerated remodeling of callus cartilage in our cKO mice could be due to the reduced IGF-I production in callus chondrocytes as the consequence of unintended deletion of the *Igf1* gene in chondrocytes.

To determine whether *Dmp1*-Cre-mediated deletion of *Igf1* in chondrocytes also occurred in chondrocytes of our cKO mutants, especially those within fracture calluses, we first performed the IHC staining for Cre on longitudinal thin sections of tibiae of 12-week-old male *Igf1* cKO mice and WT littermates for Cre protein. As shown in Suppl. Fig. S1A, there was no detectable Cre expression in chondrocytes at either the proliferative or hypertrophic zones, whereas positive Cre immunostaining was found in the few osteocytes and mature osteoblasts at the edge of the growth plate (indicated by arrows).

Our previous IHC studies have shown no obvious differences in IGF-I expression levels in either proliferating or hypertrophic chondrocytes between *Igf1* cKO mutants and WT littermates [30]. To ascertain that *Dmp1*-Cre-mediated recombination did not reduce IGF-I expression level in chondrocytes within the fracture calluses of cKO mutants, we next performed IHC for IGF-I on longitudinal thin sections of tibiae containing the fracture callus of cKO mutants and WT littermates at 7 days post-fracture (Suppl. Fig. S1B). Consistent with our previous findings of relatively low IGF-I expression in the growth plate chondrocytes [30], the *Igf1* expression level in hypertrophic chondrocytes in the healing calluses was extremely low. Also, in agreement with a previous IGF-I immunolocalization study in a rat femoral fracture study [19], IGF-I staining in both the WT and cKO fracture calluses at 7 days post-fracture was seen primarily in the proliferating chondrocytes and osteoblasts (Suppl. Fig. S1B). Importantly, because we detected no reduction in the relative amount or intensity of the IGF-I IHC staining in callus chondrocytes of cKO fracture calluses, the apparent lack of suppression effect of the *Dmp1*-Cre-mediated deletion of *Igf1* on IGF-I expression in callus chondrocytes did not support the contention that the reduced amounts and accelerated remodeling of callus cartilage-like tissues in *Igf1* cKO fractures were due to reduced expression of IGF-I in chondrocytes.

3.6. Deficient expression of Igf1 in osteocytes accelerated bone formation and bony union of fracture gap

As shown in Fig. 3C &D, the cKO fracture calluses at 21 days post-fracture had significantly higher BMD than the WT calluses, suggesting

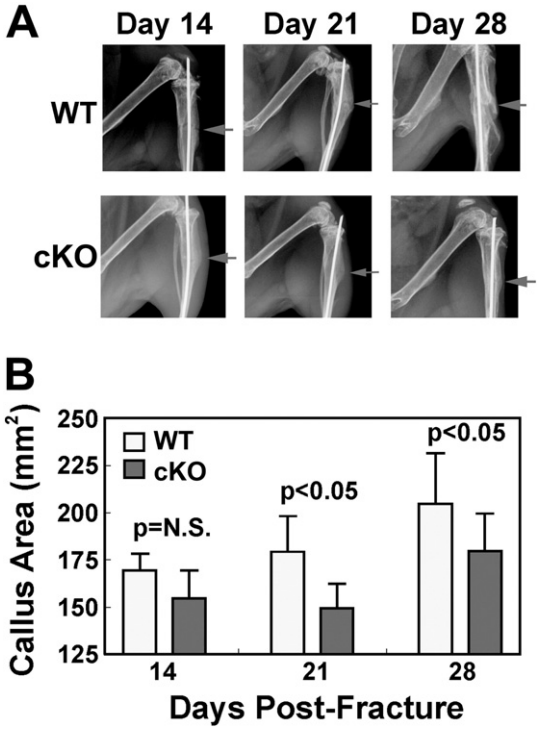

Fig. 2. Effects of deficient *Igf1* expression on the time-dependent fracture healing (A) and on the fracture callus size (B). In A, fracture healing of six *Igf1* cKO mice and six WT littermates at 14-, 21-, and 28-day post-fracture was monitored by X-ray densitometry. Five out of six of the cKO mice, but none of the six WT mice, showed X-ray evidence for bony union of the fracture gap. The fracture sites are indicated by the arrows. In B, the cross-sectional area of fracture calluses at day 14, 21, and 28 post-fracture of cKO and WT mice was measured by pQCT ($n = 6$ mice per group). N.S. = not significant ($P > 0.05$).

that cKO fractures may have significantly greater bone formation than WT fractures. To assess this possibility, we performed pQCT analyses of BMC and BMD at the fracture site of cKO mice and WT littermates at 14, 21, and 28 days post-fracture. This analysis confirms that the cKO fractures at both 21 and 28 days post-fracture (but not at 14 days) have significantly greater total BMD (t·BMD), sub-cortical (Sub–Ct·BMC) and cortical BMC (Ct·BMC), cortical bone area (Ct·B·Pm), and cortical thickness (Ct·Th) than the WT fractures (Suppl. Fig. S2).

To determine whether deficient *Igf1* expression in osteocytes would promote bony union, we next performed more detailed μ-CT scanning of bony tissues at the fracture site of cKO mice and WT littermates at 21 days post-fracture. Three-dimensional reconstruction of the fracture site showed that there were large amounts of high-density bony tissues, which covered almost the entire fracture gap of cKO mice (right panel of Fig. 6A). Similar findings were seen in all six cKO fractures. Conversely, the fracture gap of WT mice were covered mostly by low-density and apparently porous woven bony tissues (left panel of Fig. 6A). Quantitative measurements of the newly formed bone at the fracture gap confirm that cKO fracture calluses had significantly higher Tb·BV/TV than WT fracture calluses (Fig. 6B). The Tb·N was also significantly greater in cKO calluses than that in WT calluses (Fig. 6C), whereas Tb·Sp of cKO calluses was significantly lower than that in WT calluses (Fig. 6E). However, there were no significant differences in Tb·Th (Fig. 6D) or in trabecular connectivity density (Fig. 6F) between cKO and WT calluses.

We also performed torsional stiffness testing on the healing fractured tibia and contralateral intact tibia on WT littermate ($n = 7$) and cKO mutants ($n = 5$) at 21 days post-fracture. Because of the 8–12% smaller bone size in these cKO mutants [30], the basal torsional stiffness of intact contralateral tibia of cKO mice was 14% lower than WT littermates [0.0165 ± 0.002 N-mm/° (n = 5 cKO mice) vs. 0.0192 ± 0.002 N-mm/° (n = 7 WT littermates)]. Therefore, we normalized the torsional stiffness of the fractured bone against that of each corresponding contralateral intact bone to determine the return of torsional bone strength (i.e., the ratio of 1.0 would indicate a complete return of torsional bone strength). Intriguingly, the return of torsional stiffness of healing fractured tibiae of cKO mice was 37% [0.56 ± 0.17 (cKO mutants, n = 5) vs. 0.41 ± 0.09 (WT mice, n = 7)] greater than that of healing WT fractured bones. However, neither of these differences was statistically significant, since our power analysis indicated that it would require 37 mice per group to detect a 30% difference. Nonetheless, the apparent greater return of torsional stiffness is consistent with an improved fracture healing in the cKO mutants compared to corresponding WT littermates.

We next compared the mRNA levels of several osteoblastic marker genes, such as *Cbfa1* (also known as *Runx2*), alkaline phosphatase (*Alp*), osteopontin (*Opn*), and osteocalcin (*Ocn*), at the fracture site of cKO mice with those at the fracture site of WT control mice at 14 days post-fracture. Each of these genes in cKO fractures was increased two- to fourfold in expression when compared to those in WT fractures (Fig. 7), suggesting an enhanced bone formation in the cKO fractures at this time point. These findings together are consistent with our contention that the abridged endochondral bone repair process in osteocyte *Igf1* cKO fractures was attended by an increase in intramembranous bone formation that resulted in an accelerated bony union of the fracture gap.

3.7. Potential mechanism for the enhanced fracture healing in Igf1 osteocyte cKO mutant mice

To rule out the possibility that the accelerated fracture healing in cKO mutants is due to an intrinsic greater basal periosteal bone formation rate (BFR), we compared basal BFR and mineralization apposition rate (MAR) on the periosteal surface at the site corresponding to the fracture site of the intact bone of 12-week-old male cKO mice with those of age- and gender-matched WT mice. We found no significant differences in basal periosteal MAR (Fig. 8A) or in basal periosteal BFR/B·Pm (Fig. 8B) between cKO mutants and WT littermates. We have also previously determined the basal endosteal bone formation parameters of our cKO mice and corresponding age-and gender-matched WT littermates at 4 weeks or 8 weeks of age, and found that cKO mice at 8 weeks of age (but not at 4 weeks of age) exhibited ~20% reduction in tetracycline labeling surface and bone formation rate [30]. However, because the periosteum and periosteal bone formation are generally believed to be essential for the endochondral bone repair during fracture repair, and because the periosteal bone formation parameters were not significantly different between cKO and WT littermates, the observed accelerated fracture healing in cKO mutants was probably not due to intrinsic differences in basal periosteal bone formation.

There is emerging evidence that canonical Wnt signaling, which is a major anabolic pathway that stimulates bone formation [43], is involved in fracture repair [44]. Accordingly, *Sost* is a key osteocyte-derived paracrine regulatory factor that inhibit bone formation by suppressing the canonical Wnt signaling. Deficiency in *Sost* expression or functional activity, via genetic knockout [8,45] or anti-SOST antibody treatment [12,13], has been shown to promote fracture repair. Because our previous studies have reported that young adult (8-week-old) *Igf1* osteocyte cKO mutants had 40% lower basal levels of *Sost* mRNA in their bone [35], we compared the *Sost* mRNA level in the fracture callus of cKO mutants with that in WT calluses at 14 days post-fracture. The *Sost* mRNA level was slightly, but not significantly, increased in WT calluses; but it was reduced by ~50% in cKO calluses compared to the contralateral intact bone (Fig. 8C). This 50% reduction was on top of the already 40% lower basal level in the cKO mutant mice [35]. To confirm these gene expression results, we stained SOST protein by IHC on thin sections of the fracture calluses and found a drastic reduction in the SOST immunostaining (primarily inside the osteocytes) in cKO calluses compared to that in WT fracture calluses (Fig. 8E).

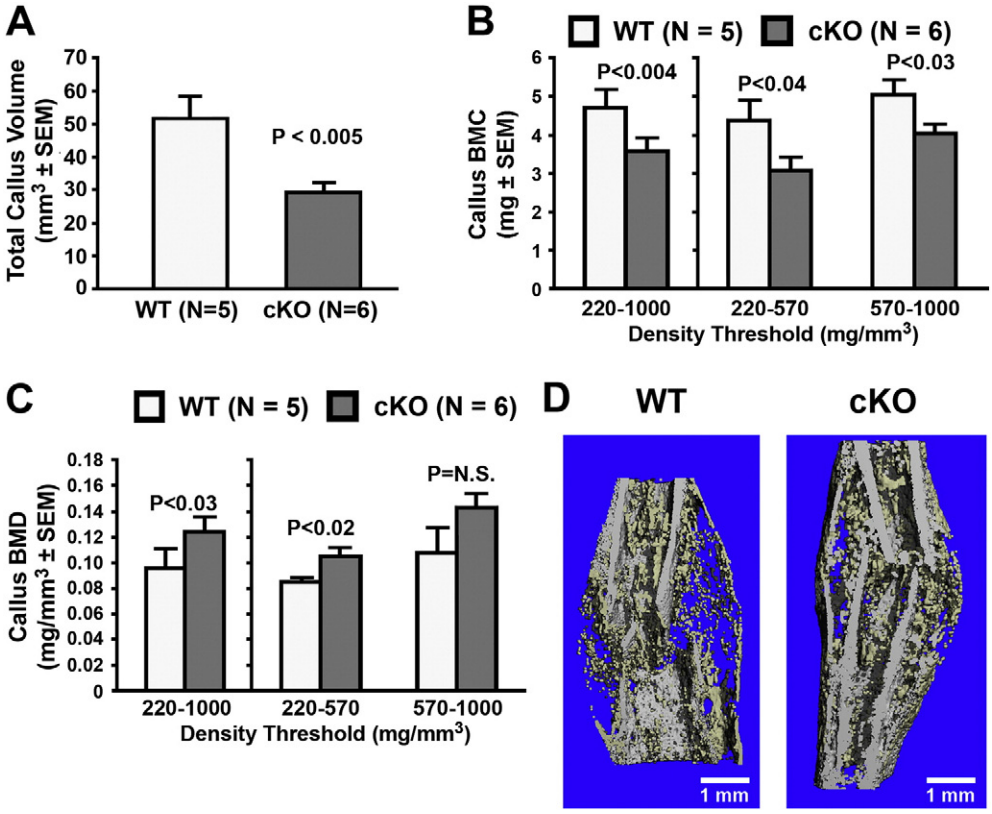

Fig. 3. Effects of deficient *Igf1* expression in osteocytes on the volume (A), bone mineral content (B), and bone mineral density (C) of the fracture calluses, and the μ-CT three-dimensional reconstruction of the longitudinal, midline cut-away view of the fracture calluses (D). In A, B, & C, the callus volume, BMC, and BMD of the healing calluses of cKO and WT mice were measured by μ-CT at 21-day post-fracture. Total callus BMC and BMD, respectively, was measured with the threshold of 220–1000 mg/mm^3. The low density, woven bone-containing callus tissues and the high density, cortical bone-containing callus tissues were each measured separately with threshold settings of 220–570 mg/mm^3 and of 570–1000 mg/mm^3, respectively. N.S. = not significant ($P > 0.05$). In D, the reconstruction of the longitudinal midline cut-away view was done on fracture calluses at 21 days post-fracture. The low density callus woven bone is shown in yellow color; whereas the high-density lamellar cortical bone is shown in white color.

It has also been reported that the fracture healing process increased expression of *Bmp2* and *Bmp4* and activated the BMP signaling in both osteoblasts and osteocytes in the newly formed bony tissue of the fracture callus [46]. The *Bmp2* expression has recently been shown to play an essential role in fracture repair [47]. The basal *Bmp2* mRNA level in bones of *Igf1* cKO mutants was not significantly different from

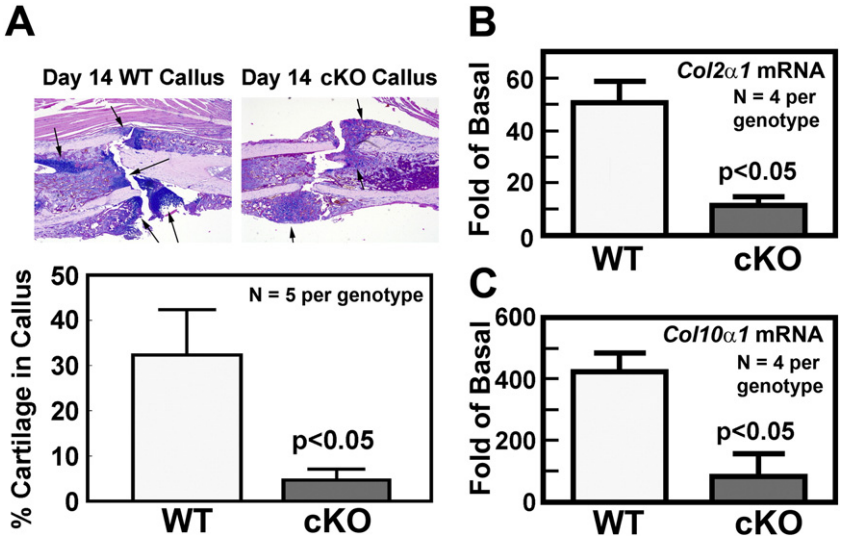

Fig. 4. Effects of deficient expression of *Igf1* in osteocytes on the relative amount of cartilage in fracture calluses at 14 days post-fracture. In A, the callus cartilage on thin longitudinal sections of the tibial facture of five cKO mice and five WT littermates was stained with Alcian blue (indicated by arrows on the top panel). Bottom panel compares the percentage of cartilage area (in relationship to the total callus area) of cKO fractures with that of WT littermates. In B & C, the relative increase in *Col2α1* mRNA *and Col10α1* mRNA, respectively, (normalized against the housekeeping gene, *Actb* mRNA) in four cKO fractures was compared with those in four WT fractures. Results are shown in relative fold of the corresponding basal level of respective mRNA species in the contralateral intact tibia.

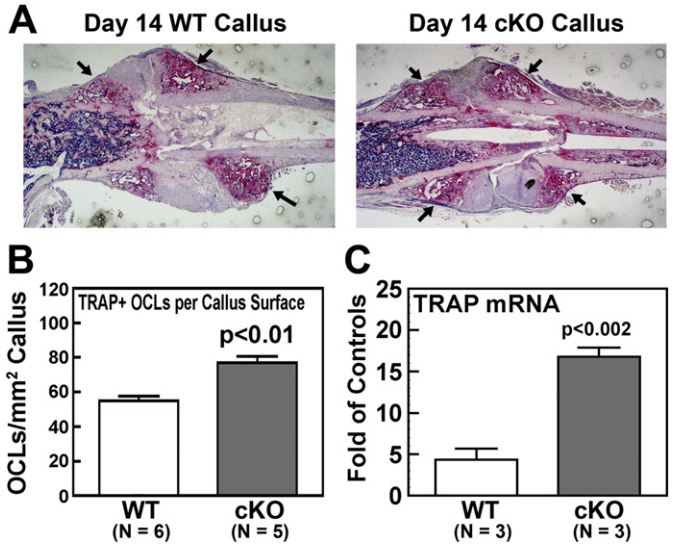

Fig. 5. Effects of deficient expression of *Igf1* in osteocytes on the TRAP-positively stained osteoclast surface (A), number of osteoclasts per callus surface (B), and TRAP mRNA expression level (C) in fracture calluses at 14 days post-fracture. In A, a representative longitudinal section of a WT fracture callus (left) and that of a cKO fracture callus (right) stained for TRAP activity are shown. TRAP-stained areas are indicated by arrows. In B, the number of TRAP-positive, multinucleated (>2 nuclei) osteoclasts on six WT fracture calluses and on five cKO fracture calluses was counted. The results are normalized against mm^2 callus surface. In C, the TRAP (*Acp5b*) mRNA (normalized against *Actb* mRNA) in the fracture calluses of three cKO mutants and of three WT littermates was measured by qRT-PCR. Results are shown as fold of the TRAP mRNA level of corresponding contralateral intact tibia control.

that in bones of WT littermates (data not shown). Importantly, at 14 days of healing, the *Bmp2* mRNA level in fracture calluses of cKO calluses was increased more than threefold compared to that in intact contralateral tibia; whereas there was no difference in the *Bmp2* mRNA level between the fractured and intact contralateral tibia of WT littermates (Fig. 8D). IHC staining of BMP2 protein confirms that there was a marked increase in BMP2 immunostaining in osteoblasts and chondrocytes within the cKO fracture callus when compared to WT fracture calluses (Fig. 8F). These findings together suggest that the enhanced fracture repair in osteocyte *Igf1* cKO mice may in part be mediated through downregulation of *Sost* expression along with upregulation of the *Bmp2* signaling at the fracture site.

4. Discussion

The total economic burden to the United States alone is approximately one billion dollars per year as a consequence of bone fractures. Accordingly, scientific advances to shorten the fracture healing time would have important consequences on both economy and patient morbidity. There is an abundance of information to suggest that the anabolic growth factor, IGF-I, would accelerate fracture healing [16,19,21,22] and that osteocytes play an essential role in fracture healing [6,8,15]. We undertook the present study to test the hypothesis that osteocyte-derived IGF-I plays an enhancing role in the fracture repair process by evaluating the consequence of conditional deletion of *Igf1* in osteocytes on the healing of tibial fractures in mice. Of all the disciplines of biology, the one that produces the most unexpected results is genetics. This study with the osteocyte *Igf1* cKO mice fulfilled that prophecy. Accordingly, we did not find an impaired fracture healing in our cKO mice as expected. Even more surprising was the finding that the fracture healing as assessed by the valid criterion (i.e., bony union of the fracture gap) was actually accelerated. These surprising results were reproducible and were confirmed in repeat experiments. Bony union is a valid histological surrogate of fracture healing. Thus, it appears that conditional deletion of *Igf1* in osteocytes not only did not impede, but in fact unexpectedly accelerated, fracture healing. We should also note that although IGF-I is known to be essential for normal cartilage growth and development, the reduced formation of the cartilaginous callus and the accelerated fracture repair seen in cKO mutants were probably not due to reduction in local production of chondrocyte-derived IGF-I in fracture calluses, since there was no apparent reduction in the IGF-I expression in fracture callus chondrocytes between osteocyte *Igf1* cKO mutants and corresponding WT littermates (Suppl. Fig. S1B).

This surprising but exciting result provided us with a unique opportunity. The disruption of a single gene (i.e., *Igf1*) in a single cell type (i.e., osteocyte) that provided a positive effect on fracture healing has the potential to disclose important healing mechanisms for future therapeutic targeting. We previously introduced the concept that it would be an advantage to have fracture healing by intramembranous bone formation as opposed to endochondral bone formation, because it would eliminate the cartilage formation phase and thereby accelerates bony union [2]. This concept was based in part on our observations that the Cox-2 gene therapy of fractures accelerated bony union, and it did so by shortening the endochondral bone formation process along with an increase in intramembranous bone formation [33]. Our concept is also supported by recent findings that activation of Wnt signaling, either through inhibition of GSK3 [48] or via deletion of Wnt inhibitory genes (*Sost* [9] or *sFrp1* [49]), promoted fracture healing and accelerated bony union through enhancing intramembranous bone formation and at the same time curtailing endochondral bone formation. In the present study, we found strong suggestive evidence that targeted disruption of *Igf1* alone in osteocytes appeared to shift the fracture healing process from a slower endochondral process to the more rapid intramembranous process. In this regard, the intramembranous process is obviously characterized by less cartilage-like tissues, which was found in the present study (Fig. 4). Additionally, intramembranous bone repair yields a smaller callus, which was again documented in the present study (Fig. 2). Incidentally, the Cox-2 gene therapy, which favors intramembranous bone formation over endochondral bone formation, also yielded smaller cartilaginous calluses [33].

From the foregoing, it would appear that the acceleration of bony union of the fracture gap in our mouse tibial fracture model was due to a shift from endochondral toward intramembranous bone formation. The molecular mechanisms responsible for this shift are not entirely clear; however, there are data, which allow us to make tenable explanations for this shift. A pivotal clue generated from this study with respect to our proposed mechanism in which the fracture of osteocyte *Igf1* cKO mutant mice was healed primarily through the intramembranous bone formation was the highly significant, 50% reduction in *Sost* expression (Fig. 8). *Sost* is a potent inhibitor of the canonical Wnt signaling, which has shown to be essential for fracture repair [50,51]. It is reasonable to assume that the canonical Wnt signaling at the fracture site was activated in our cKO mutant mouse. In this regard, activation of Wnt signaling has been shown to promote fracture healing through primarily intramembranous bone formation [8–14].

It is particularly interesting that Wnt signaling favors osteogenesis and tends to inhibit chondrogenesis [9,45,48]. This would be consistent with our finding that our cKO mutant mouse expresses phenotypic features of intramembranous bone formation in contrast with the control mouse. That there was an increase in intramembranous bone formation is firmly established by elevated expression levels of bone formation marker genes, including Cbfa1, alkaline phosphatase, osteocalcin, and osteopontin (Fig. 7). The latter parameters are a measure of differentiated cell function, and in this regard, we found >3-fold increase in *Bmp2* mRNA and protein expression in osteoblasts and chondrocytes within the fracture callus. Both Wnts and BMPs are thought to be essential mediators of fracture healing [44,47]. However, the mechanism for the essential increase in the *Bmp2* expression during fracture healing has not been established. This is probably a local mechanism in the local milieu, and not a consequence of the Wnt signaling per se. This is a consistent fact that when signaling promotes cell proliferation in the intestinal crypt, this process is followed by a decrease in *Wnt* expression and an

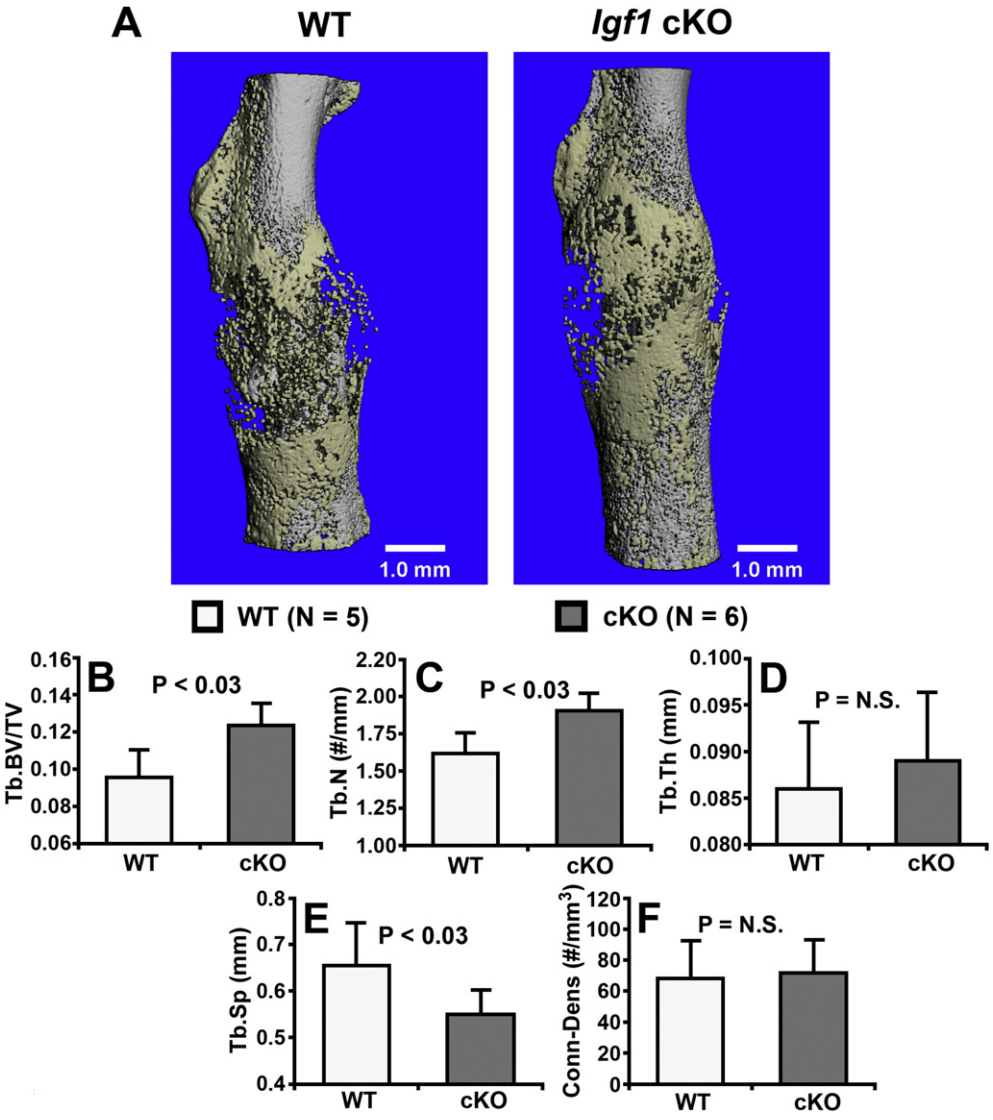

Fig. 6. Effects of deficient expression of *Igf1* in osteocytes on the μ-CT trabecular bone parameters at the fracture site at 21 days post-fracture. Panel A shows the three-dimensional reconstruction of the fracture site of a representative cKO mutant and that of a representative WT littermate. Panels B–F compare the trabecular bone volume (tb·BV/TV), number (Tb·N), thickness (Tb·Th), spacing (Tb·Sp), and connectivity density (Conn-Dens), respectively, inside fracture calluses of six *Igf1* osteocyte cKO mutants with those inside fracture calluses of five WT littermates. N.S. = not significant ($P > 0.05$).

increase in *Bmp* expression, which promotes differentiation of the crypt cells [52,53]. Although the exact mechanisms for the increase in *Bmp2* expression during fracture healing in our cKO mice require further study, we have incorporated the BMP2 signaling in our model of the mechanism for the shift of endochondral bone formation to intramembranous bone formation, which is described in detail in Suppl. Fig. S3.

In this model, we postulate that the bone fracture induces the surviving osteocytes to secrete IGF-I during the early healing phase in WT animals [19]. The secreted osteocyte-derived IGF-I then acts as an autocrine factor to increase osteocytic production and release of *Sost* and at the same time as a paracrine factor on nearby bone cells to suppress *Bmp2* expression. Consistent with this premise is the previous finding of large increases of sclerostin protein in the fracture hematoma of patients with bone fractures [54]. This would then lead to downregulation of the Wnt and BMP2 signaling, respectively (indicated by the dashed arrows in Suppl. Fig. S3A). The coordinated downregulation of Wnt and BMP2 signaling during early healing phases would allow for a precise and balanced regulation of the differentiation of MSCs (recruited to the fracture site during early healing phases [2]) to favor chondrocytic differentiation. This precise regulation of MSC differentiation is critical for an optimal endochondral bone formation required for formation of a functional cartilaginous callus [44]. At later phases of the healing, the amount of the released osteocyte-derived IGF-I is drastically reduced [19], resulting in a marked reduction in local *Sost* expression and the corresponding upregulation of the canonical Wnt signaling. This premise is supported by the significant reduction in *Sost* expression in fracture callus at later healing phases [7]. The Wnt signaling would then act on osteoblasts to promote intramembranous bone formation, leading to bony union of the fracture gap. In osteocyte *Igf1* cKO mutant mice (Suppl. Fig. S3B), deficient expression of osteocyte-derived IGF-I drastically reduces the local concentration of sclerostin and increases BMP2 level, which then led to upregulation of the Wnt signaling in MSCs and osteoblasts, and the BMP2 signaling in MSCs, osteoblasts, and osteoclasts. During early healing phases, the upregulation of the Wnt and BMP2 signaling in MSCs shifted the MSC differentiation to favor osteoblastic over chondrocytic differentiation, leading to the suppression of formation of cartilage-like tissues at the fracture gap. The sustained activation of the Wnt and BMP2 signaling at the later healing phases would then work together to speed up intramembranous bone formation to complete the union of the fracture gap. An additional complementary mechanism in the process of fracture repair, which was

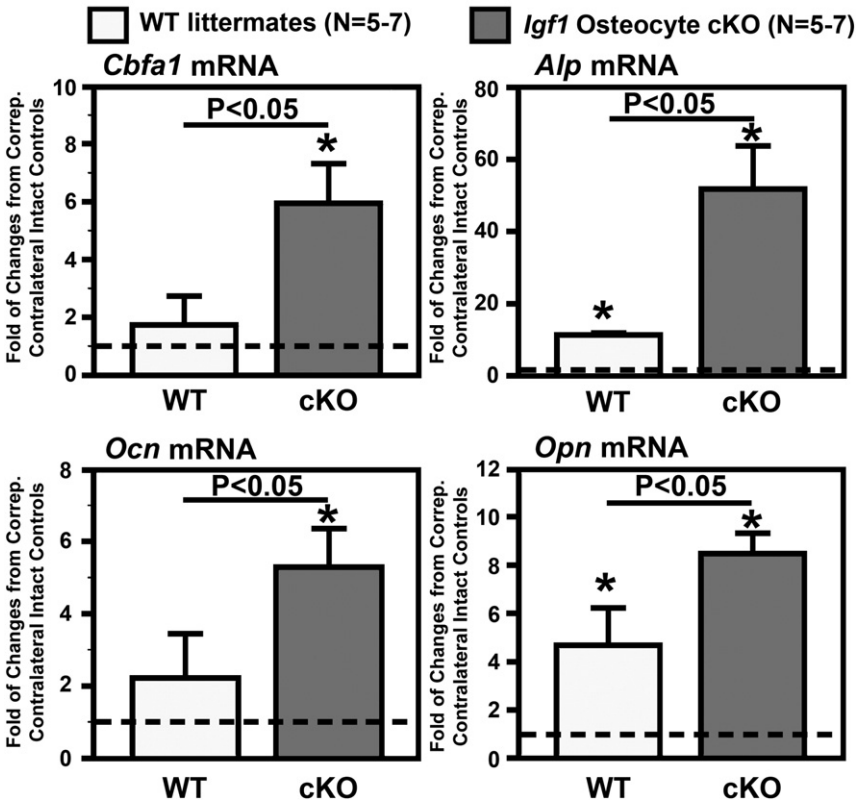

Fig. 7. Effects of deficient expression of *Igf1* in osteocytes on the relative expression level of *Cbfa1*, *Alp*, *Ocn*, and *Opn* mRNA in fracture calluses at 14 days post-fracture. The bone containing the entire fracture callus was isolated from cKO mice or corresponding WT mice at14 days post-fracture. Total mRNA was isolated and reversed transcribed to cDNA. The mRNA levels of respective osteoblastic genes were determined by qPCR and normalized against each corresponding level of *Actb* mRNA. Results are shown as the relative fold of changes from the basal level of corresponding contralateral intact tibia (mean ± SEM). The dashed line in each panel represents the corresponding basal level (i.e., 1-fold) of each indicated gene. *P < 0.05, compared to corresponding basal levels.

accelerated in our cKO mutant mouse model, was an increase in remodeling of the fracture callus during the later phases of the healing process. That there was an actual increase in remodeling of cartilaginous callus is based on decreased measurements of callus size vs control between 14 and 28 days of healing time (Fig. 2), which was attended by increases in osteoclast number and TRAP (*Acp5b*) mRNA expression (Fig. 5). Because BMP2 can activate osteoclasts directly or indirectly [55,56], the increases in osteoclast number and activity may be mediated through BMP2 (Suppl. Fig. S3). In addition, the mechanism by which osteocyte-derived IGF-I regulates osteocytic *Sost* expression is unclear and will be the subject of future studies. We do know that osteocyte IGF-I expression changes substantially during fracture repair with very high expression levels early on and then a gradual progressive decline [18,19], but it remains to be determined as to whether this mirrors the activation of Wnt signaling during fracture repair.

We should also note that the histology and morphology of the cartilage-like tissues in cKO fractures at 7 days (Suppl. Fig. S1B) or 14 days (Fig. 8F) post-fracture appeared to be different from those of the cartilage tissues in WT calluses, in that the cartilage tissues in cKO calluses were stained much weaker for proteoglycans (Fig. 4A), expressed significantly less type II and X collagens (Fig. 4B&C), and contained fewer numbers of hypertrophic chondrocytes (Suppl. Fig. S1B), than WT calluses. The reason for this apparent difference in the cartilage histology and morphology is unclear. On the one hand, because it is our premise that deficient expression of *Igf1* in osteocytes accelerates fracture healing, we speculate that the relative healing stage of the cKO fracture callus at any given time point is comparatively more advanced than that of corresponding WT fractures. Accordingly, we suggest that the apparent differences in the cartilage histology may simply reflect the more advanced healing stage in cKO fractures compared to WT fractures at each time point. Relevant to this speculation is the finding that conditional disruption of *Igf1* in osteocytes not only did not diminish, but in fact increased, the IGF-I expression in the cKO fracture callus at 7 days post-fracture (Suppl. Fig. S1B). Since the cKO fractures healed much faster than WT fractures, we propose that the healing stage of the cKO fractures at 7 days post-fracture might be equivalent to that of the WT fractures at 14 days of post-fracture or later. In this regard, since a previous study of differential gene expression and immunolocalization of IGFs in a rat femoral fracture model has shown a time-dependent increase in IGF-I expression in the fracture callus with healing [19], the higher IGF-I expression level seen in cKO calluses than in WT calluses at 7 days post-fracture could be due to a more advanced stage of the healing. In the future, we will confirm this speculation with a time-course study. If our speculation is confirmed, this would lend further support for our argument that the apparent difference in cartilage histology between cKO and WT fracture calluses reflects the more advanced healing stage in cKO fractures than in WT fractures.

On the other hand, conditional deletion of *Igf1* in osteocytes could also affect the cellular or molecular process of the fracture healing, which could then lead to the formation of a different type of callus cartilage (e.g., some form of "primordial" cartilage-like soft tissues) in the cKO fractures. This type of "primordial" cartilage-like tissue may then permit an accelerated angiogenic invasion into the soft callus mass in a manner akin to that occurring in the hypertrophic zone of growth plate cartilage, which may speed up the endochondral remodeling and the subsequent acceleration in bony bridging of the fracture gap. This alternative mechanism has merits and cannot be ruled out. Consequently, our future studies will evaluate this alternative mechanism by characterizing the cartilage-like soft tissues in cKO mutant mice and determining their role in the accelerated fracture repair in cKO mutant mice.

In summary, our model describes the concept that a deficiency of osteocyte-derived IGF-I leads to a decrease in SOST production, which in

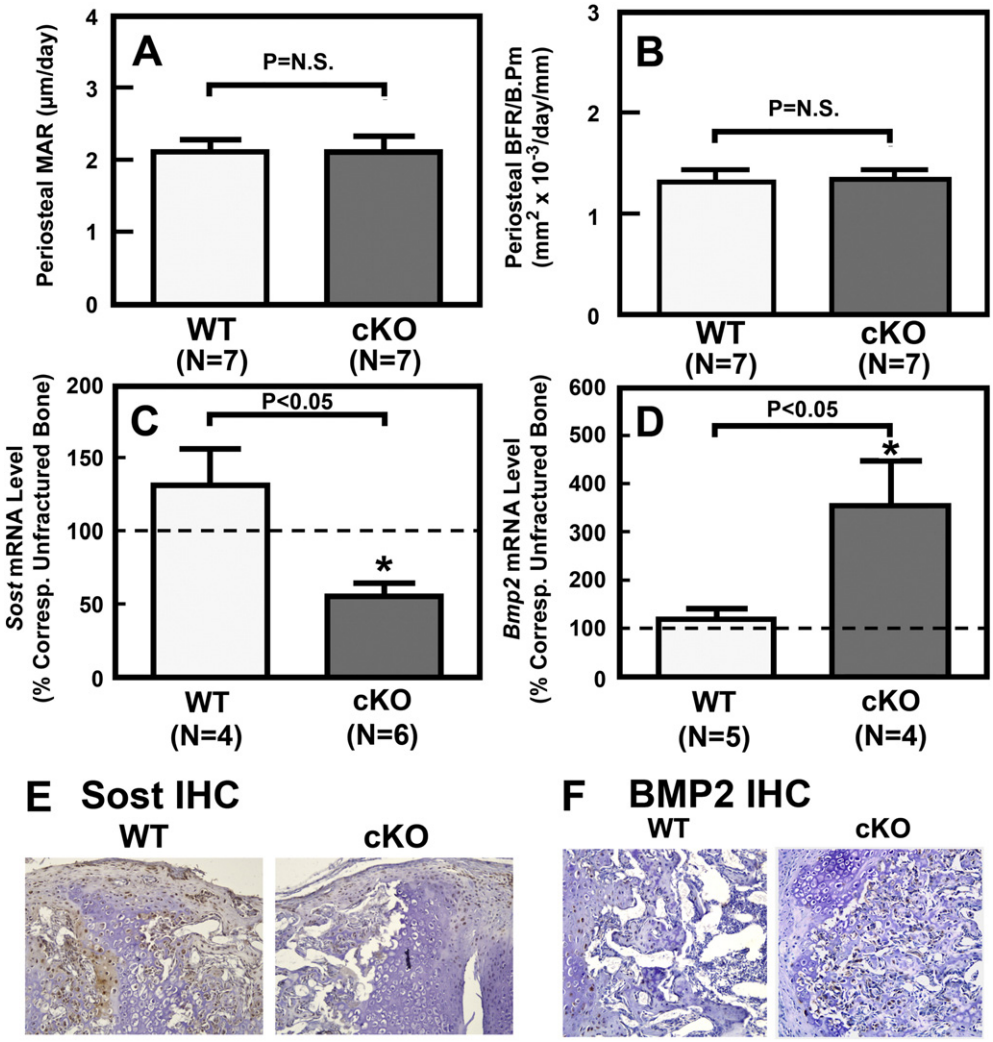

Fig. 8. Effects of deficient expression of *Igf1* in osteocytes on the basal periosteal mineral apposition rate (A), basal periosteal bone formation rate per bone surface (B), on the relative expression level of *Sost* mRNA (C) and *Bmp2* mRNA (D), and on IHC staining of Sost (E) and BMP2 (F), respectively, in calluses at 14 days post-fracture. In A & B, basal periosteal MAR and BFR/B·Pm were determined in 12-week-old male cKO mice and corresponding WT littermates before fracture by dynamic bone histomorphometry. In C and D, the *Sost* and *Bmp2* mRNA levels (normalized against *Actb* mRNA) were determined by qPCR. Results are shown as the relative fold of changes from the basal level of corresponding contralateral intact tibia (mean ± SEM). The dashed line in each panel represents the corresponding basal level (i.e., 1-fold) of each indicated gene. *$P < 0.05$, compared to corresponding basal levels. N.S. = not significant ($P > 0.05$). In E and F, IHC was performed on longitudinal thin sections of the fracture calluses, and the IHC staining for a representative fracture each of osteocyte *Igf1* cKO mutant mice and corresponding WT littermates.

turn increases the canonical Wnt signaling. This signaling process creates a milieu resulting in increased expression of BMP2, which together with the Wnt signaling promotes intramembranous over endochondral bone formation, reflected by a smaller callus and less cartilage. This occurs during the early process of fracture healing. Additionally, there is an accelerating later phase of fracture healing characterized by increased bone remodeling (increased formation and resorption) to result in fracture union and restoration of bone strength. In conclusion, we have discovered a novel mechanism, which can normally lead to a shift from slowly progressing endochondral bone formation to rapidly progressing intramembranous bone formation attended by an increase in bone strength. The existence of this mechanistic process was heretofore unknown to occur. Further studies will be required to test several aspects of our proposed conceptual model.

Acknowledgements

This work was supported by the Telemedicine and Advanced Technology Research Center (TATRC) at the US Army Medical Research and Material Command (USAMRMC) under Grant # W81XWH-08-1-0697. The views, opinions and/or findings contained in this report are those of the authors and should not be construed as an official Department of the Army position, policy or decision unless so designated by other documentation. The authors thank Prof. Derek LeRoith for the generous gift of the *Igf1*$^{flox/flox}$ breeding pair and acknowledge the excellent technical assistance of Ms. Denise Galvan.

Appendix A. Supplementary data

Supplementary data to this article can be found online at http://dx.doi.org/10.1016/j.bone.2016.08.005.

References

[1] M.E. Bolander, Regulation of fracture repair by growth factors, Proc. Soc. Exp. Biol. Med. 200 (1992) 165–170.
[2] K.H. Lau, V. Kothari, A. Das, X.B. Zhang, D.J. Baylink, Cellular and molecular mechanisms of accelerated fracture healing by COX2 gene therapy: studies in a mouse model of multiple fractures, Bone 53 (2013) 369–381.

[3] L.F. Bonewald, The amazing osteocyte, J. Bone Miner. Res. 26 (2011) 229–238.
[4] H. Kamioka, T. Honjo, T. Takano-Yamamoto, A three-dimensional distribution of osteocyte processes revealed by the combination of confocal laser scanning microscopy and differential interference contrast microscopy, Bone 28 (2001) 145–149.
[5] K. Hirakawa, S. Hirota, T. Ikeda, A. Yamaguchi, T. Takemura, J. Nagoshi, et al., Localization of the mRNA for bone matrix proteins during fracture healing as determined by in situ hybridization, J. Bone Miner. Res. 9 (1994) 1551–1557.
[6] M. Li, N. Amizuka, K. Oda, K. Tokunaga, T. Ito, K. Takeuchi, et al., Histochemical evidence of the initial chondrogenesis and osteogenesis in the periosteum of a rib fractured model: implications of osteocyte involvement in periosteal chondrogenesis, Microsc. Res. Tech. 64 (2004) 330–342.
[7] J. Caetano-Lopes, A. Lopes, A. Rodrigues, D. Fernandes, I.P. Perpetuo, T. Monjardino, et al., Upregulation of inflammatory genes and downregulation of sclerostin gene expression are key elements in the early phase of fragility fracture healing, PLoS One 6 (2011), e16947.
[8] C. Li, M.S. Ominsky, H.L. Tan, M. Barrero, Q.T. Niu, F.J. Asuncion, et al., Increased callus mass and enhanced strength during fracture healing in mice lacking the sclerostin gene, Bone 49 (2011) 1178–1185.
[9] M.E. McGee-Lawrence, Z.C. Ryan, L.R. Carpio, S. Kakar, J.J. Westendorf, R. Kumar, Sclerostin deficient mice rapidly heal bone defects by activating beta-catenin and increasing intramembranous ossification, Biochem. Biophys. Res. Commun. 441 (2013) 886–890.
[10] L. Cui, H. Cheng, C. Song, C. Li, W.S. Simonet, H.Z. Ke, et al., Time-dependent effects of sclerostin antibody on a mouse fracture healing model, J Musculoskelet Neuronal Interact 13 (2013) 178–184.
[11] M.U. Jawad, K.E. Fritton, T. Ma, P.G. Ren, S.B. Goodman, H.Z. Ke, et al., Effects of sclerostin antibody on healing of a non-critical size femoral bone defect, J. Orthop. Res. 31 (2013) 155–163.
[12] G. Feng, Z. Chang-Qing, C. Yi-Min, L. Xiao-Lin, Systemic administration of sclerostin monoclonal antibody accelerates fracture healing in the femoral osteotomy model of young rats, Int. Immunopharmacol. 24 (2015) 7–13.
[13] P.K. Suen, Y.X. He, D.H. Chow, L. Huang, C. Li, H.Z. Ke, et al., Sclerostin monoclonal antibody enhanced bone fracture healing in an open osteotomy model in rats, J. Orthop. Res. 32 (2014) 997–1005.
[14] C.S. Yee, L. Xie, S. Hatsell, N. Hum, D. Murugesh, A.N. Economides, et al., Sclerostin antibody treatment improves fracture outcomes in a type I diabetic mouse model, Bone 82 (2016) 122–134.
[15] A.E. Loiselle, E.M. Paul, G.S. Lewis, H.J. Donahue, Osteoblast and osteocyte-specific loss of Connexin43 results in delayed bone formation and healing during murine fracture healing, J. Orthop. Res. 31 (2013) 147–154.
[16] M. Ellegaard, T. Kringelbach, S. Syberg, S. Petersen, J.E. Beck Jensen, A. Bruel, et al., The effect of PTH(1–34) on fracture healing during different loading conditions, J. Bone Miner. Res. 28 (2013) 2145–2155.
[17] L. Meinel, E. Zoidis, J. Zapf, P. Hassa, M.O. Hottiger, J.A. Auer, et al., Localized insulin-like growth factor I delivery to enhance new bone formation, Bone 33 (2003) 660–672.
[18] A. Igarashi, M. Yamaguchi, Increase in bone growth factors with healing rat fractures: the enhancing effect of zinc, Int. J. Mol. Med. 8 (2001) 433–438.
[19] A. Koh, T. Niikura, S.Y. Lee, K. Oe, T. Koga, Y. Dogaki, et al., Differential gene expression and immunolocalization of insulin-like growth factors and insulin-like growth factor binding proteins between experimental nonunions and standard healing fractures, J. Orthop. Res. 29 (2011) 1820–1826.
[20] Y. Rhee, M.R. Allen, K. Condon, V. Lezcano, A.C. Ronda, C. Galli, et al., PTH receptor signaling in osteocytes governs periosteal bone formation and intracortical remodeling, J. Bone Miner. Res. 26 (2011) 1035–1046.
[21] A. Nakajima, N. Shimoji, K. Shiomi, S. Shimizu, H. Moriya, T.A. Einhorn, et al., Mechanisms for the enhancement of fracture healing in rats treated with intermittent low-dose human parathyroid hormone (1–34), J. Bone Miner. Res. 17 (2002) 2038–2047.
[22] G. Schmidmaier, B. Wildemann, T. Gabelein, J. Heeger, F. Kandziora, N.P. Haas, et al., Synergistic effect of IGF-I and TGF-beta1 on fracture healing in rats: single versus combined application of IGF-I and TGF-beta1, Acta Orthop. Scand. 74 (2003) 604–610.
[23] F.H. Shen, J.M. Visger, G. Balian, S.R. Hurwitz, D.R. Diduch, Systemically administered mesenchymal stromal cells transduced with insulin-like growth factor-I localize to a fracture site and potentiate healing, J. Orthop. Trauma 16 (2002) 651–659.
[24] D.G. Xing, Z.H. Liu, H.W. Gao, W.L. Ma, L. Nie, M.Z. Gong, Effect of transplantation of marrow mesenchymal stem cells transfected with insulin-like growth factor-1 gene on fracture healing of rats with diabetes, Bratisl. Lek. Listy 116 (2015) 64–68.
[25] S. Larsson, W. Kim, V.L. Caja, E.L. Egger, N. Inoue, E.Y. Chao, Effect of early axial dynamization on tibial bone healing: a study in dogs, Clin. Orthop. Relat. Res. 240-51 (2001).
[26] J. Kenwright, J.B. Richardson, J.L. Cunningham, S.H. White, A.E. Goodship, M.A. Adams, et al., Axial movement and tibial fractures. A controlled randomised trial of treatment, J. Bone Joint Surg. (Br.) 73 (1991) 654–659.
[27] P. Augat, U. Simon, A. Liedert, L. Claes, Mechanics and mechano-biology of fracture healing in normal and osteoporotic bone, Osteoporos. Int. 16 (Suppl. 2) (2005) S36–S43.
[28] A.K. Ulstrup, Biomechanical concepts of fracture healing in weight-bearing long bones, Acta Orthop. Belg. 74 (2008) 291–302.
[29] K.H. Lau, D.J. Baylink, X.D. Zhou, D. Rodriguez, L.F. Bonewald, Z. Li, et al., Osteocyte-derived insulin-like growth factor I is essential for determining bone mechanosensitivity, Am. J. Physiol. Endocrinol. Metab. 305 (2013) E271–E281.
[30] M.H. Sheng, X.D. Zhou, L.F. Bonewald, D.J. Baylink, K.H. Lau, Disruption of the insulin-like growth factor-1 gene in osteocytes impairs developmental bone growth in mice, Bone 52 (2013) 133–144.
[31] F. Bonnarens, T.A. Einhorn, Production of a standard closed fracture in laboratory animal bone, J. Orthop. Res. 2 (1984) 97–101.
[32] C.H. Rundle, N. Miyakoshi, Y. Kasukawa, S.T. Chen, M.H. Sheng, J.E. Wergedal, et al., In vivo bone formation in fracture repair induced by direct retroviral-based gene therapy with bone morphogenetic protein-4, Bone 32 (2003) 591–601.
[33] C.H. Rundle, D.D. Strong, S.T. Chen, T.A. Linkhart, M.H. Sheng, J.E. Wergedal, et al., Retroviral-based gene therapy with cyclooxygenase-2 promotes the union of bony callus tissues and accelerates fracture healing in the rat, J Gene Med 10 (2008) 229–241.
[34] M.H. Sheng, D.J. Baylink, W.G. Beamer, L.R. Donahue, C.J. Rosen, K.H. Lau, et al., Histomorphometric studies show that bone formation and bone mineral apposition rates are greater in C3H/HeJ (high-density) than C57BL/6J (low-density) mice during growth, Bone 25 (1999) 421–429.
[35] K.H. Lau, D.J. Baylink, M.H. Sheng, Osteocyte-derived insulin-like growth factor I is not essential for the bone repletion response in mice, PLoS One 10 (2015), e0115897.
[36] Z. Xiao, M. Dallas, N. Qiu, D. Nicolella, L. Cao, M. Johnson, et al., Conditional deletion of Pkd1 in osteocytes disrupts skeletal mechanosensing in mice, FASEB J. 25 (2011) 2418–2432.
[37] M. Sinnesael, F. Claessens, M. Laurent, V. Dubois, S. Boonen, L. Deboel, et al., Androgen receptor (AR) in osteocytes is important for the maintenance of male skeletal integrity: evidence from targeted AR disruption in mouse osteocytes, J. Bone Miner. Res. 27 (2012) 2535–2543.
[38] I. Kramer, S. Baertschi, C. Halleux, H. Keller, M. Kneissel, Mef2c deletion in osteocytes results in increased bone mass, J. Bone Miner. Res. 27 (2012) 360–373.
[39] S.H. Windahl, A.E. Borjesson, H.H. Farman, C. Engdahl, S. Moverare-Skrtic, K. Sjogren, et al., Estrogen receptor-alpha in osteocytes is important for trabecular bone formation in male mice, Proc. Natl. Acad. Sci. U. S. A. 110 (2013) 2294–2299.
[40] B. Javaheri, A.R. Stern, N. Lara, M. Dallas, H. Zhao, Y. Liu, et al., Deletion of a single beta-catenin allele in osteocytes abolishes the bone anabolic response to loading, J. Bone Miner. Res. 29 (2014) 705–715.
[41] E.L. Clinkenbeard, T.A. Cass, P. Ni, J.M. Hum, T. Bellido, M.R. Allen, et al., Conditional deletion of murine Fgf23: Interruption of the normal skeletal responses to phosphate challenge and rescue of genetic hypophosphatemia, J. Bone Miner. Res. 31 (2016) 1247–1257.
[42] S. Chen, J. Feng, Q. Bao, A. Li, B. Zhang, Y. Shen, et al., Adverse effects of osteocytic constitutive activation of ss-catenin on bone strength and bone growth, J. Bone Miner. Res. 30 (2015) 1184–1194.
[43] X. Li, Y. Zhang, H. Kang, W. Liu, P. Liu, J. Zhang, et al., Sclerostin binds to LRP5/6 and antagonizes canonical Wnt signaling, J. Biol. Chem. 280 (2005) 19883–19887.
[44] Y. Chen, H.C. Whetstone, A.C. Lin, P. Nadesan, Q. Wei, R. Poon, et al., Beta-catenin signaling plays a disparate role in different phases of fracture repair: implications for therapy to improve bone healing, PLoS Med. 4 (2007), e249.
[45] A. Morse, N.Y. Yu, L. Peacock, K. Mikulec, I. Kramer, M. Kneissel, et al., Endochondral fracture healing with external fixation in the Sost knockout mouse results in earlier fibrocartilage callus removal and increased bone volume fraction and strength, Bone 71 (2015) 155–163.
[46] Y.Y. Yu, S. Lieu, C. Lu, T. Miclau, R.S. Marcucio, C. Colnot, Immunolocalization of BMPs, BMP antagonists, receptors, and effectors during fracture repair, Bone 46 (2009) 841–851.
[47] T.J. Myers, L. Longobardi, H. Willcockson, J.D. Temple, L. Tagliafierro, P. Ye, et al., BMP2 regulation of CXCL12 cellular, temporal, and spatial expression is essential during fracture repair, J. Bone Miner. Res. 30 (2015) 2014–2027.
[48] G. Sisask, R. Marsell, A. Sundgren-Andersson, S. Larsson, O. Nilsson, O. Ljunggren, et al., Rats treated with AZD2858, a GSK3 inhibitor, heal fractures rapidly without endochondral bone formation, Bone 54 (2013) 126–132.
[49] T. Gaur, J.J. Wixted, S. Hussain, S.L. O'Connell, E.F. Morgan, D.C. Ayers, et al., Secreted frizzled related protein 1 is a target to improve fracture healing, J. Cell. Physiol. 220 (2009) 174–181.
[50] E.E. Beier, T.J. Sheu, T. Buckley, K. Yukata, R. O'Keefe, M.J. Zuscik, et al., Inhibition of β-catenin signaling by Pb leads to incomplete fracture healing, J. Orthop. Res. 32 (2014) 1397–1405.
[51] Y. Huang, X. Zhang, K. Du, F. Yang, Y. Shi, J. Huang, et al., Inhibition of beta-catenin signaling in chondrocytes induces delayed fracture healing in mice, J. Orthop. Res. 30 (2012) 304–310.
[52] T.M. Yeung, L.A. Chia, C.M. Kosinski, C.J. Kuo, Regulation of self-renewal and differentiation by the intestinal stem cell niche, Cell. Mol. Life Sci. 68 (2011) 2513–2523.
[53] B. Han, S.Y. Chen, Y.T. Zhu, S.C. Tseng, Integration of BMP/Wnt signaling to control clonal growth of limbal epithelial progenitor cells by niche cells, Stem Cell Res. 12 (2014) 562–573.
[54] K. Sarahrudi, A. Thomas, C. Albrecht, S. Aharinejad, Strongly enhanced levels of sclerostin during human fracture healing, J. Orthop. Res. 30 (2012) 1549–1555.
[55] E.D. Jensen, L. Pham, C.J. Billington Jr., K. Espe, A.E. Carlson, J.J. Westendorf, et al., Bone morphogenic protein 2 directly enhances differentiation of murine osteoclast precursors, J. Cell. Biochem. 109 (2010) 672–682.
[56] K. Tachi, M. Takami, B. Zhao, A. Mochizuki, A. Yamada, Y. Miyamoto, et al., Bone morphogenetic protein 2 enhances mouse osteoclast differentiation via increased levels of receptor activator of NF-kappaB ligand expression in osteoblasts, Cell Tissue Res. 342 (2010) 213–220.